The Astrophysical Journal, 680:1072–1082, 2008 June 20

Lyα-EMITTING GALAXIES AT $0.2 < z < 0.35$ FROM *GALEX* SPECTROSCOPY

Jean-Michel Deharveng,[1] Todd Small,[2] Tom A. Barlow,[2] Céline Péroux,[1] Bruno Milliard,[1] Peter G. Friedman,[2] D. Christopher Martin,[2] Patrick Morrissey,[2] David Schiminovich,[3] Karl Forster,[2] Mark Seibert,[2] Ted K. Wyder,[2] Luciana Bianchi,[4] Jose Donas,[1] Timothy M. Heckman,[5] Young-Wook Lee,[6] Barry F. Madore,[7] Susan G. Neff,[8] R. Michael Rich,[9] Alex S. Szalay,[5] Barry Y. Welsh,[10] and Sukyoung K. Yi[6]

Received 2007 November 5; accepted 2008 March 1

ABSTRACT

We have used the *GALEX* (*Galaxy Evolution Explorer*) spectroscopic survey mode, with a resolution of ~8 Å in the far-ultraviolet (FUV; 1350–1750 Å) and ~20 Å in the near-ultraviolet (NUV; 1950–2750 Å) for a systematic search of Lyα-emitting galaxies at low redshift. Our aim is to fill a gap between high-redshift surveys and a small set of objects studied in detail in the nearby universe. A blind search of 7018 spectra extracted in five deep exposures (5.65 deg^2) has resulted in 96 Lyα-emitting galaxy candidates in the FUV domain after accounting for broad-line AGNs. The Lyα equivalent widths (EWs) are consistent with stellar population model predictions and show no trends as a function of UV color or UV luminosity, with the exception of a possible decrease in the most luminous objects that may be due to small-number statistics. The objects' distribution in EW is similar to that at $z \sim 3$, but their fraction among star-forming galaxies is smaller. Avoiding uncertain candidates, a subsample of 66 objects in the range $0.2 < z < 0.35$ has been used to build a Lyα luminosity function (LF). The incompleteness due to objects with significant Lyα emission but a UV continuum too low for spectral extraction has been evaluated. A comparison with Hα LFs in the same redshift domain is consistent with an average Lyα/Hα of ~1 in about 15% of the star-forming galaxies. A comparison with high-redshift Lyα LFs implies an increase of the Lyα luminosity density by a factor of about 16 from $z \sim 0.3$ to $z \sim 3$. By comparison with the factor of 5 increase in the UV luminosity density in the same redshift range, this suggests an increase of the average Lyα escape fraction with redshift.

Subject headings: galaxies: evolution — galaxies: ISM — galaxies: luminosity function, mass function — galaxies: starburst — ultraviolet: galaxies

1. INTRODUCTION

The Lyα emission line has attracted great attention as a spectral signature useful for identifying galaxies and securing redshifts at large distances. Use of this emission line, however, is fraught with difficulty. Because Lyα photons are resonantly scattered by neutral hydrogen, they may suffer more dust attenuation than adjacent UV continuum photons; their escape is also affected by the relative geometries of neutral and ionized interstellar gas, and last but not least by the velocity structure of neutral gas. The first two factors have been extensively discussed in light of *IUE* observations of nearby star-forming galaxies (Giavalisco et al. 1996 and references therein) and with model calculations (Charlot & Fall 1993; Neufeld 1991; Chen & Neufeld 1994 and references therein). The crucial role of the velocity structure of neutral gas has been shown by the *Hubble Space Telescope* (*HST*) spectra of nearby star-forming galaxies (Kunth et al. 1998; Mas-Hesse et al. 2003). Similar evidence was offered by the spectra of Lyman break galaxies (LBGs; Pettini et al. 1998, 2000). Lyα photons mainly escape when they are scattered off neutral gas that is offset in velocity from the bulk of the ionized regions. The complexity of the escape of Lyα emission is also well illustrated by the broad distribution of Lyα strengths and profile types observed in the LBG spectroscopic sample of Shapley et al. (2003). The Lyα transmission mechanisms, especially the resulting emergent line profiles, have since been investigated in increasingly realistic models (e.g., Ahn et al. 2001, 2002, 2003; Hansen & Oh 2006; Verhamme et al. 2006). An extensive review of all the aspects of the observations of the Lyα emission line in galaxies has recently been given by Schaerer (2007).

The complex nature of Lyα escape has been blamed for the disappointing results of earlier searches of distant Lyα emitters (e.g., Djorgovski & Thompson 1992). Nonetheless, the Lyα emission remains the only means of identifying galaxies when the continuum becomes too faint to be detected. Following Cowie & Hu (1998) and Hu et al. (1998), ever deeper and larger surveys have come into widespread use for detecting galaxies at high redshifts. Beyond $z \sim 6$, the increasingly neutral intergalactic medium (IGM) is not a complete obstacle to the visibility of Lyα emission (e.g., Haiman 2002), and the density evolution of Lyα emitters may even help to trace the history of cosmic reionization (e.g., Malhotra & Rhoads 2004; Stern et al. 2005; Kashikawa et al. 2006).

Although nearby galaxies have played a key role in understanding the factors affecting Lyα escape, their observations, using space-borne UV spectrographs in pointing mode, were directed

[1] Laboratoire d'Astrophysique de Marseille, UMR 6110 CNRS/Université de Provence, BP 8, Traverse du Siphon, 13376 Marseille Cedex 12, France.
[2] California Institute of Technology, MC 405-47, 1200 East California Boulevard, Pasadena, CA 91125.
[3] Department of Astronomy, Columbia University, New York, NY 10027.
[4] Center for Astrophysical Sciences, The Johns Hopkins University, 3400 North Charles Street, Baltimore, MD 21218.
[5] Department of Physics and Astronomy, The Johns Hopkins University, Homewood Campus, Baltimore, MD 21218.
[6] Center for Space Astrophysics, Yonsei University, Seoul 120-749, Korea.
[7] Observatories of the Carnegie Institution of Washington, 813 Santa Barbara Street, Pasadena, CA 91101.
[8] Laboratory for Astronomy and Solar Physics, NASA Goddard Space Flight Center, Greenbelt, MD 20771.
[9] Department of Physics and Astronomy, University of California, Los Angeles, CA 90095.
[10] Space Sciences Laboratory, University of California, 601 Campbell Hall, Berkeley, CA 94720.

TABLE 1
CHARACTERISTICS OF THE FIVE *GALEX* SPECTROSCOPIC FIELDS USED

Parameter	CDFS-00	ELAISS1-00	GROTH-00	NGPDWS-00	SIRTFFL-00
Exposure time (s)	149315	84086	281713	139598	79616
Center of field R.A.[a]	53.128	9.638	214.992	219.156	259.124
Center of field decl.[a]	−27.871	−43.990	52.782	35.171	59.909
Identified sources[b]	38697	30129	43545	40619	28306
Extracted spectra	1419	925	2028	1202	1444
Emission features	22	9	39	19	7
Used for the LF[c]	15	5	29	11	6

[a] In decimal degrees.
[b] Entries in the matched catalog of the FUV and NUV images.
[c] Used for the evaluation of the LF.

toward specific and known objects. As a consequence, there is not yet a systematic survey for redshifts smaller than those reachable from the ground. Here, we use the *GALEX* spectroscopic survey mode for the first systematic search of Lyα-emitting galaxies at low redshift. Our goals are to understand (1) whether the Lyα escape is related to specific properties of galaxies and (2) whether the Lyα emission evolves from current epoch to high z in step with the cosmic star formation rate traced by Balmer lines or the UV continuum of galaxies. If so, the average relationship between the massive stellar content of the galaxies and their Lyα emission would be constant over time, and the Lyα emission might be used as a tracer of star formation, with an empirical calibration encapsulating the average effects of resonant scattering. If not, there would be evidence for cosmic evolution of the physical processes, especially galactic winds, which are expected to play a central role in the Lyα escape from galaxies.

2. DATA ANALYSIS

2.1. *GALEX Ultraviolet Spectroscopy and Selection of Line Emitters*

The *GALEX* instrument and mission are described by Martin et al. (2005) and Morrissey et al. (2005). The spectroscopy mode utilizes a CaF_2 grism that can be moved into the convergent beam of the telescope to form simultaneous spectra of all sources in the field in both far-ultraviolet (FUV) and near-ultraviolet (NUV) bands. The usable wavelength range for relatively faint sources is approximately 1350–1750 Å for FUV (second order) and 1950–2750 Å for NUV (first order). The spectral resolution for a point source (assuming a 5″ point-spread function) is ∼8 Å for FUV and ∼20 Å for NUV. Details on the observations (multiple grism orientations in order to avoid overlapping spectra) and the various steps of data reduction are given by Morrissey et al. (2007). The spectral extraction is performed for all point sources in the direct image observations exceeding a signal-to-noise ratio (S/N) limit per resolution element in the coadded results of 2 in FUV and 3 in NUV. Each resulting spectrum is a one-line image of 488 pixels, with 3.5 Å per pixel and starting at 1300 Å.

Eleven fields observed in spectroscopy mode are available from the *GALEX* GR2 data release. In order to keep a relative homogeneity in the detection depth and related selection effects, we have concentrated on five fields with an exposure time longer than 70,000 s and covering an area of 5.65 deg^2. The characteristics of these five fields are summarized in Table 1, with the total number of spectra extracted by the reduction pipeline and the number of objects identified in the same fields with the direct imaging mode. Each spectrum has been visually inspected, and potential Lyα emission features (central wavelength, line flux, equivalent width, and full width at half-maximum [FWHM]) have been measured with the IRAF `splot` package (Gaussian fitting). The S/N does not permit reasonable identifications of Lyα absorption.

The objects with a FWHM larger than about 15 Å in the FUV domain and about 27 Å in the NUV are classified as broad-line AGNs. These limits are based on a minimum value of 1200 km s^{-1}, observed in the distribution of the FWHM of the Hα emission line of galaxies in the Sloan Digital Sky Survey (SDSS; Hao et al. 2005a) and found to make a separation between the broad-line AGNs and other emission-line objects. These limits take into account the average redshift and the spectral resolution in the respective *GALEX* UV bands. The presence/absence of emission lines such as O VI, C III, and C IV, when the redshift is appropriate and the brightness large enough for detection in the *GALEX* bands, is also used to confirm the classification, especially when the FWHM values are close to the limit values.

In the NUV domain, only broad-line AGNs are found according to our criteria. This is consistent with the NUV (AB) limiting magnitude of 22 of the vast majority of extracted spectra. At a redshift of 0.65, the lowest redshift at which a Lyα emitter can be detected in the NUV band, this flux limit would imply an (AB) absolute magnitude brighter than −21, a value extreme and rare for galaxies, as shown by the evolution of the galaxy 1500 Å luminosity function (Arnouts et al. 2005). This situation is aggravated by the dilution of narrow spectral features into the ∼20 Å NUV spectral resolution, which plays against the detection of Lyα-emitting galaxies.

We have found it impossible to identify narrow-line AGNs among our potential Lyα-emitting galaxies, because either their associated C IV line is redshifted into the noisy wavelength domain between the FUV and NUV, or the object is too faint for a detection of the C III or C IV lines. A contamination by narrow-line AGNs is probably present, and it will be seen in the next subsection whether additional spectral information can help.

As our blind search was open to all extracted spectra and not limited to galaxies with appropriate redshift, we have an increased risk of spurious detections. We have therefore classified our candidates into three categories (1=good, 2=fair, and 3=uncertain) in order to try to monitor whether the properties of our objects depend on the quality of their identification, even though the sample sizes are changing. Figure 1 gives a few examples of these spectra with the proposed identification. The identification of potential Lyα features is also hampered at both ends of the spectral range by fluctuations that increase because of the decrease in efficiency. In between, the useful spectral range is not constant from object to object. For the problems that require a control of the volume

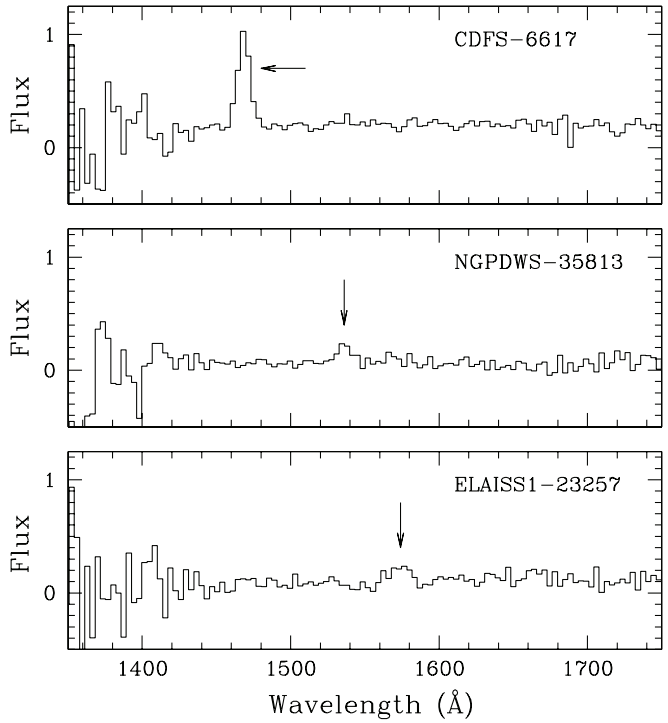

FIG. 1.—Examples of *GALEX* spectra (in flux units of 10^{-4} photons cm^{-2} s^{-1} Å^{-1}) and features identified (*from top to bottom*) as Lyα emission with qualities good ($Q = 1$), fair ($Q = 2$), and uncertain ($Q = 3$).

surveyed, we have defined the largest wavelength domain that we have been able to search in relatively uniform conditions for all the objects. This wavelength range of 1459–1642 Å translates into a redshift window of 0.2–0.35 for the Lyα emission line.

The number of Lyα emission-line candidates resulting from our blind search, as well as those retained for the discussion of luminosity functions (qualities 1 and 2 only; $0.2 < z < 0.35$) are listed in Table 1 for each field investigated. The total numbers are 96 and 66, respectively, in these two categories. Table 2 summarizes the main characteristics of our candidates with the line flux of the emission features, and, assuming an identification with Lyα emission, the redshift and the derived Lyα luminosity. The line fluxes and Lyα luminosities include a correction factor resulting from a recalibration of the spectral response, which was determined to make no systematic differences, on average, between the direct image photometry and the fluxes derived from an integration of the spectra. The 1 σ precision on the line-flux measurement is on the order of 4×10^{-16} erg cm^{-2} s^{-1}. In combination with an evaluation of the uncertainty in the determination of the UV continuum adjacent to the emission line, this number gives a precision on the equivalent width (EW) from about 25% at EW $\sim$ 20 Å to 15% at EW $\sim$ 100 Å.

2.2. *Cross-Verification with Spectroscopic or Photometric Redshift Information*

As a control on our blind search, we have compared our results with existing information about each candidate, especially any redshift from spectroscopy or photometry in the optical. We are mostly concerned with spurious features, and not confusion with another emission line, since Lyα emission is known to be unique in the FUV spectra of galaxies. The possibility of identifying narrow-line AGNs would also be of interest, since we have shown it to be difficult to achieve in practice with the UV spectra alone.

Each of our 96 candidates was searched in the NASA/IPAC Extragalactic Database (NED) and the recent Data Release 3 of DEEP2 (Davis et al. 2007); the 14 redshifts found are displayed in Table 2. Only one of these redshifts, based on COMBO-17 photometric measurements (Wolf et al. 2004) and possibly affected by misidentification in a dense group, is in significant disagreement with the evaluation based on the Lyα emission. All 14 objects are classified as galaxies. Although this cross-verification is presently limited to a small subset of the candidates, it is seen as an encouraging validation of our approach. The small number of redshifts available from the visible was somewhat expected. On the one hand, the SDSS spectroscopic survey (available in three of our five fields) has a small fraction of galaxies at $z > 0.2$; on the other hand, the *GALEX* spectroscopy is not deep enough to overlap well the specific and deep-redshift surveys with large telescopes.

3. PROPERTIES OF THE Lyα-EMITTING GALAXIES

3.1. *Comparison with the UV-selected Galaxy Population*

We compared our Lyα-emitting galaxy candidates with the other UV sources of *GALEX*, especially those identified as galaxies, in order to see whether the presence of the Lyα line is related to any galaxy property. Such a comparison can also illustrate the importance of selection effects. In the plot of the FUV flux versus UV color, the 96 Lyα-emitting candidates lie at the faint-magnitude and blue-color boundaries of the domain occupied by the 736 objects classified as galaxies but without Lyα features. Our candidates' presence near the faint-magnitude boundary is easy to explain, since in principle they lie at redshift $z > 0.2$. The blue-color boundary has two possible explanations. On the one hand, easier Lyα escape may accompany less dust and bluer color; on the other hand, bluer color may imply a higher FUV continuum flux and easier detection of emitting features.

Another aspect of the comparison of our Lyα-emitting candidates with respect to the general population of *GALEX* sources is shown in Figure 2 in the distribution of the FUV magnitudes. This distribution is displayed for four samples: the UV sources detected in the images, the extracted spectra, the objects classified as galaxies (without any emission feature), and the Lyα-emitting galaxy candidates. The spectra appear to have been systematically extracted down to a magnitude of 21.5, a level at which samples are complete according to the completeness analysis of *GALEX* images by Xu et al. (2005). The distribution of objects classified as galaxies also peaks at this limit. At the bright end of the distribution, the proportion of galaxies with Lyα emission is naturally low, since the objects are selected at $z > 0.2$. At the faint end, the number of objects classified as galaxies and the number of Lyα-emitting galaxy candidates are very similar. This does not mean that all identified faint galaxies have Lyα in emission, since the samples are distinct by construction, but it tells us that the identification of faint galaxies is relatively easier with an emission feature than without one. The distribution of Lyα-emitting galaxy candidates peaks at magnitudes in the range 21.5–22. They are clearly affected by incompleteness.

3.2. *Distribution of Lyα EW*

The distribution of Lyα rest-frame equivalent widths is displayed in Figure 3. Beyond a completeness limit at about 20 Å, the distribution is comparable with that of Shapley et al. (2003) for LBGs at $z \sim 3$. The fraction of Lyα-emitting galaxies (with EW > 20 Å) relative to the number of star-forming galaxies in the redshift range $0.2 < z < 0.35$ cannot be determined directly, because redshift measurements are available only in limited areas,

TABLE 2

THE Lyα-EMITTING GALAXY CANDIDATES

Field (1)	ID (2)	R.A. (deg) (3)	Decl. (deg) (4)	EW (Å) (5)	Q (6)	Lyα Flux (10^{-15} erg cm^{-2} s^{-1}) (7)	FUV (8)	Color (9)	z (10)	log $L_{\mathrm{Ly}\alpha}$ (erg s^{-1}) (11)	Lit. z[a] (12)
CDFS.....	1348	53.2405	−28.3883	43.4	1	5.43	21.35	0.615	0.217	41.87	
CDFS.....	1821	53.2585	−28.3577	24.6	1	3.37	21.30	0.303	0.251	41.81	
CDFS.....	2422	52.8947	−28.3395	14.4	2	4.79	20.54	0.488	0.176	41.63	0.1728 (1)
CDFS.....	3801	52.7375	−28.2794	29.7	1	3.62	21.55	0.528	0.285	41.97	
CDFS.....	4927	52.9765	−28.2386	102.	1	8.12	21.89	0.450	0.283	42.31	
CDFS.....	5007	53.5412	−28.2554	97.7	2	3.14	22.74	1.283	0.344	42.09	
CDFS.....	5448	53.0780	−28.2224	149.	1	11.4	21.42	0.312	0.283	42.46	
CDFS.....	6523	53.0616	−28.1865	47.4	1	3.48	21.70	0.551	0.264	41.87	
CDFS.....	6535	52.9622	−28.1890	34.8	1	5.16	21.01	0.386	0.216	41.85	
CDFS.....	6617	53.1743	−28.1903	50.9	1	17.2	20.19	−0.037	0.208	42.33	
CDFS.....	7100	52.9993	−28.1644	29.1	1	2.96	21.42	0.282	0.239	41.71	
CDFS.....	10526	53.5868	−28.0657	24.3	1	1.75	22.11	0.940	0.361	41.89	
CDFS.....	10937	53.7850	−28.0454	63.0	1	5.89	21.41	0.423	0.346	42.37	
CDFS.....	11518	53.0498	−28.0250	57.7	1	5.50	21.72	0.249	0.218	41.89	0.212 (2)
CDFS.....	16104	53.2360	−27.8879	23.2	2	4.35	21.14	0.544	0.374	42.32	0.365 (3)
CDFS.....	17033	52.7601	−27.8584	38.1	3	3.57	21.96	0.494	0.340	42.14	
CDFS.....	18142	52.8861	−27.8344	24.4	2	4.63	21.04	0.052	0.183	41.64	0.133 (2)
CDFS.....	19355	53.7296	−27.8008	28.7	1	7.49	20.56	0.783	0.314	42.38	
CDFS.....	21667	53.2803	−27.7424	11.8	2	2.50	20.77	0.506	0.219	41.55	0.216 (4)
CDFS.....	21739	53.7113	−27.7293	34.8	1	4.05	21.56	0.731	0.323	42.14	
CDFS.....	30899	53.3592	−27.4543	78.6	1	7.29	21.63	0.502	0.352	42.48	
CDFS.....	33311	53.1045	−27.2904	58.0	1	8.65	21.43	0.271	0.391	42.66	
ELAISS1	13715	9.6383	−44.0090	21.9	3	2.93	21.64	1.308	0.213	41.59	
ELAISS1	16998	9.5205	−43.8745	56.9	1	8.16	21.11	0.508	0.223	42.08	
ELAISS1	6587	9.5590	−44.2436	102.	1	17.9	21.14	−0.107	0.272	42.62	
ELAISS1	8180	9.8839	−44.1917	38.2	2	10.1	20.34	0.881	0.188	42.01	0.1862 (5)
ELAISS1	21062	9.6663	−43.7225	12.5	2	2.81	21.13	0.204	0.211	41.56	
ELAISS1	23257	9.4752	−43.6410	32.7	3	5.17	21.34	0.512	0.294	42.15	
ELAISS1	23425	9.3711	−43.6356	21.1	2	6.49	20.87	0.387	0.300	42.27	
ELAISS1	16921	10.2733	−43.8748	20.3	3	4.14	21.53	0.929	0.312	42.12	
ELAISS1	2386	10.0078	−44.4288	32.8	2	2.81	21.94	0.732	0.268	41.80	
GROTH.....	6834	215.6564	52.4520	11.1	2	2.01	21.26	0.466	0.197	41.35	
GROTH.....	32462	215.1704	53.1138	20.8	2	1.61	21.49	0.442	0.202	41.28	0.2004 (6)
GROTH.....	36896	214.9730	53.3764	29.4	1	3.29	21.14	0.373	0.199	41.57	
GROTH.....	7430	214.4311	52.4683	104.6	1	7.67	21.80	−0.101	0.211	42.00	0.2092 (7)
GROTH.....	5087	214.5594	52.3956	44.6	3	1.23	22.61	0.746	0.215	41.22	
GROTH.....	34512	214.2955	53.1980	70.2	1	5.44	21.29	2.580	0.215	41.87	0.2139 (6)
GROTH.....	8885	215.6107	52.5075	42.4	2	2.45	21.94	0.379	0.221	41.55	
GROTH.....	2368	214.5933	52.3067	54.2	2	1.89	22.35	0.655	0.242	41.52	
GROTH.....	18322	214.5216	52.7522	25.8	2	2.78	21.63	0.335	0.247	41.71	0.24438 (8)
GROTH.....	2682	214.7013	52.2986	19.3	3	1.52	22.03	0.370	0.244	41.44	
GROTH.....	5715	214.2262	52.4111	27.7	1	3.59	21.51	0.507	0.250	41.83	0.24678 (8)
GROTH.....	19002	214.4387	52.7719	59.9	1	2.94	22.09	0.265	0.248	41.74	0.24419 (8)
GROTH.....	17005	215.1805	52.7188	26.0	2	2.87	21.59	0.304	0.252	41.74	
GROTH.....	4719	214.8114	52.3908	25.3	3	1.42	22.16	0.394	0.257	41.46	
GROTH.....	20285	215.1330	52.7994	30.9	1	4.11	21.13	0.401	0.256	41.92	
GROTH.....	21404	215.1861	52.8351	25.3	1	2.53	21.64	0.290	0.256	41.70	
GROTH.....	12279	214.3008	52.5991	19.6	2	2.08	21.76	0.527	0.264	41.65	0.26113 (8)
GROTH.....	14069	215.3526	52.6555	29.0	2	1.80	22.28	0.463	0.260	41.57	
GROTH.....	21024	214.7318	52.8245	41.0	2	2.01	21.13	−0.026	0.269	41.65	0.2633 (6)
GROTH.....	36336	214.5818	53.3393	40.3	3	2.24	22.29	1.265	0.268	41.70	
GROTH.....	37457	214.7951	53.2660	90.7	1	4.38	21.90	0.925	0.266	41.98	
GROTH.....	3488	214.9704	52.3502	40.4	2	2.52	21.83	0.541	0.269	41.75	
GROTH.....	37380	215.1904	53.3248	26.1	2	1.93	21.70	0.472	0.269	41.64	
GROTH.....	3525	214.7796	52.3522	55.2	2	2.41	22.15	0.766	0.271	41.74	
GROTH.....	29573	214.8762	53.0349	23.9	3	1.32	22.05	0.586	0.271	41.48	
GROTH.....	31403	214.2910	53.0867	33.5	1	2.25	21.86	0.570	0.270	41.71	
GROTH.....	33559	214.9025	53.1601	23.0	2	1.77	22.02	0.377	0.273	41.61	
GROTH.....	17867	215.8429	52.7425	22.0	3	1.21	22.36	0.621	0.282	41.48	
GROTH.....	17525	215.8241	52.7135	31.9	3	2.62	21.77	0.756	0.283	41.82	
GROTH.....	9045	214.9070	52.5070	24.5	2	1.86	21.75	0.475	0.286	41.68	
GROTH.....	15686	215.9047	52.6719	26.6	2	2.21	21.73	0.461	0.287	41.76	
GROTH.....	13305	215.8867	52.6237	24.6	3	1.70	21.96	0.471	0.286	41.64	

TABLE 2—*Continued*

Field (1)	ID (2)	R.A. (deg) (3)	Decl. (deg) (4)	EW (Å) (5)	Q (6)	Lyα Flux (10^{-15} erg cm^{-2} s^{-1}) (7)	FUV (8)	Color (9)	z (10)	log $L_{Ly\alpha}$ (erg s^{-1}) (11)	Lit. z[a] (12)
GROTH.....	21579	214.2081	52.8388	31.1	2	1.71	21.99	0.501	0.287	41.65	
GROTH.....	28751	214.7328	52.9926	42.5	1	2.92	21.88	0.509	0.290	41.89	
GROTH.....	23096	215.5339	52.8738	70.4	1	3.80	22.52	1.220	0.307	42.06	
GROTH.....	29558	214.0695	53.0259	65.7	2	2.58	22.18	1.077	0.329	41.96	
GROTH.....	19364	215.7761	52.7797	45.3	1	2.67	22.01	0.681	0.347	42.04	
GROTH.....	5549	215.4769	52.4065	28.3	2	4.24	21.22	0.832	0.350	42.24	
GROTH.....	10182	214.3223	52.5384	55.7	3	4.89	21.85	0.354	0.461	42.59	
NGPDWS.....	28760	219.1979	35.4351	115.0	1	20.66	20.93	0.061	0.180	42.27	
NGPDWS.....	23216	218.6954	35.2844	34.0	1	4.09	21.42	0.543	0.192	41.63	
NGPDWS.....	32840	219.2433	35.5977	20.9	2	2.32	21.46	0.771	0.209	41.47	
NGPDWS.....	11927	219.1004	34.9935	48.9	1	4.34	21.57	0.267	0.216	41.77	
NGPDWS.....	19918	219.1990	35.1757	26.2	3	3.74	21.13	0.711	0.253	41.86	
NGPDWS.....	23690	219.8446	35.3075	41.2	1	5.88	21.12	0.150	0.250	42.05	
NGPDWS.....	28521	219.0262	35.4586	23.9	1	4.05	21.57	0.189	0.253	41.90	
NGPDWS.....	35813	219.0558	35.7291	30.4	2	3.70	21.47	0.084	0.263	41.90	
NGPDWS.....	33782	219.5770	35.6305	78.2	1	6.05	21.63	0.521	0.264	42.11	
NGPDWS.....	10002	219.0922	34.9421	30.8	1	4.33	21.47	0.312	0.272	42.00	
NGPDWS.....	6731	219.1529	34.8428	51.7	1	10.10	21.15	0.496	0.283	42.41	
NGPDWS.....	2111	219.3562	34.6855	35.3	1	3.67	21.64	0.641	0.292	42.00	
NGPDWS.....	30997	218.7306	35.5246	19.4	2	3.13	21.11	0.523	0.320	42.02	
NGPDWS.....	1133	219.1333	34.6415	153.0	3	4.86	22.46	1.074	0.358	42.33	
NGPDWS.....	27558	219.1931	35.4176	117.0	3	6.02	22.20	0.993	0.372	42.46	
NGPDWS.....	10713	219.7463	34.9603	69.3	3	5.16	21.94	0.647	0.374	42.40	
NGPDWS.....	6321	219.7806	34.8359	77.2	3	7.43	22.32	0.944	0.374	42.55	
NGPDWS.....	35880	219.2820	35.6919	161.0	3	4.69	22.79	1.859	0.468	42.58	
NGPDWS.....	4226	219.3340	34.7577	56.0	1	6.49	21.53	0.350	0.328	42.36	
SIRTFFL	14450	259.2110	59.9642	41.8	1	22.19	19.77	0.133	0.185	42.33	
SIRTFFL	14297	258.6840	59.9474	28.4	2	2.52	21.62	0.494	0.219	41.55	
SIRTFFL	14085	258.1492	59.9468	15.8	2	2.87	20.99	0.624	0.225	41.63	
SIRTFFL	10895	258.5918	59.8333	49.5	1	6.18	21.28	0.192	0.233	42.00	
SIRTFFL	958	258.8205	59.3897	30.2	2	3.45	21.03	0.547	0.235	41.76	
SIRTFFL	4246	259.8606	59.5599	49.9	2	3.58	21.57	0.556	0.237	41.78	
SIRTFFL	2856	259.3800	59.4875	33.6	2	4.72	20.94	0.610	0.302	42.14	

NOTES.—Col. (5): Lyα equivalent width. Col. (6): Quality of the detection (1=good; 2=fair; 3=uncertain). Col. (7): Emission-line flux. Col. (8): FUV magnitude (in the AB system) from *GALEX* photometry. Col. (9): FUV − NUV color from *GALEX* photometry. Col. (10): Redshift assuming that the emission feature is Lyα. Col. (11): Lyα luminosity. Col. (12): Redshift found in the literature (NED) and references.

[a] Redshifts from literature/NED: (1) 2dF (http://www.mso.anu.edu.au/2dFGRS/); (2) COMBO-17, Wolf et al. 2004; (3) Vanzella et al. 2006; (4) SARS, Way et al. 2005; (5) LCRS, Shectman et al. 1996; (6) SDSS; (7) DEEP1 Groth Strip, Weiner et al. 2005; (8) DEEP2 Data Release 3, Davis et al. 2007.

and in these areas the number of matches with *GALEX* spectra is very small. We can rely on evaluations based on the *GALEX* far-UV survey and use the luminosity function (LF) derived by Arnouts et al. (2005) in the redshift range $0.2 < z < 0.4$ to calculate the total number of galaxies up to a given magnitude in a volume comparable to our observed volume. Up to magnitudes (AB) of 21 and 21.5, the numbers of Lyα-emitting galaxies with EW > 20 Å are respectively 9 (out of 58) and 36 (out of 243), corresponding to a fraction of 15% of the total number of (star-forming) galaxies. This fraction is lower than the fraction of 25% reported by Shapley et al. (2003) for LBGs at $z \sim 3$. This difference may reflect differences between the methods of evaluation. The spectroscopic sample of Shapley et al. (2003) does not have a UV flux limit such as we had to use for the determination of the size of the parent population, since our candidates are sought among objects of unknown redshifts. On the other hand, the difference is consistent with the trend of lower incidence of Lyα emission at low redshift found by Reddy et al. (2008); they, however, report a fast decline in the fraction of Lyα-emitting galaxies (EW > 20 Å), with a value of 8% in the redshift bin $1.9 < z < 2.17$.

The Lyα rest-frame EWs displayed in Figure 3 are consistent with the large spread of values predicted by the stellar population models of Charlot & Fall (1993) and any amount of Lyα quenching in the resonant scattering process. EW values larger than model predictions, which raise problems at high redshift (Shimasaku et al. 2006; Finkelstein et al. 2007; Stanway et al. 2007), are not found.

3.3. *Lyα Dependences: GALEX Data*

We also examine how the Lyα strength varies across our sample as a function of different galaxy parameters. The most obvious parameters are those relative to the UV continuum emission as obtained from *GALEX* photometry, which have the advantage of being available for all our candidates.

The variation of the Lyα rest-frame EW as a function of the UV color does not show any trend (Fig. 4). Insofar as the UV color reflects the continuum extinction, this is consistent with a decoupling of the reddening of line and continuum photons in the resonant scattering process. This is in contrast with the trend reported by Shapley et al. (2003) of the EW increasing as the UV continuum slope becomes bluer. Their trend, however, encompasses a much wider range of EWs than ours, from strong

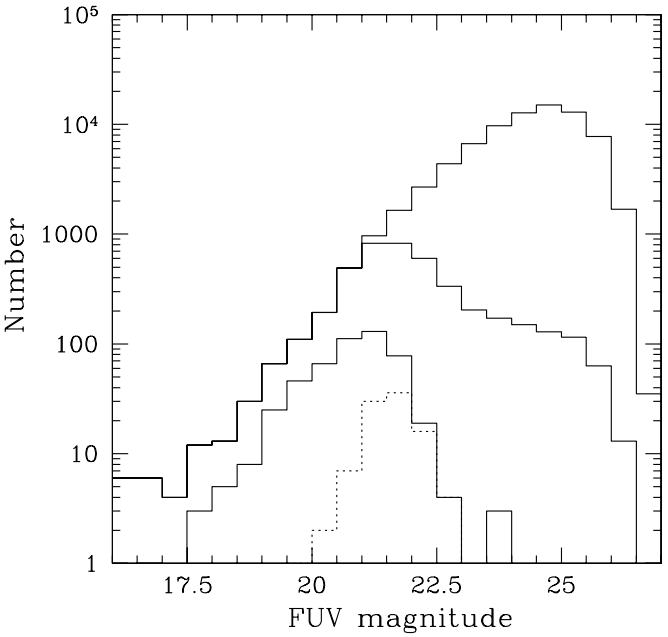

FIG. 2.—Distribution of FUV (AB) magnitudes (all five fields selected). The solid lines (*from top to bottom*) represent sources detected in the images, sources with an extracted spectrum, and sources classified as galaxies. The dotted line represents the Lyα-emitting galaxy candidates.

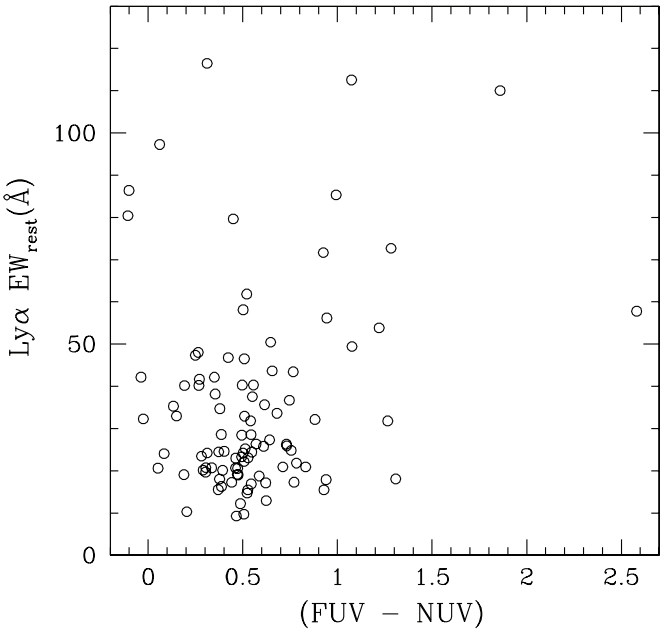

FIG. 4.—Lyα rest-frame EW as a function of the (FUV − NUV) color.

absorption to strong emission, and would be less significant if restricted to our limited range of EWs.

The Lyα rest-frame EW also reveals no trend as a function of the UV luminosity (Fig. 5). The deficiency of strong Lyα emission reported in the most luminous high-z LBGs (Ando et al. 2004, 2006; Shimasaku et al. 2006) is not directly comparable, since it takes place at an absolute magnitude <-21, a limit that we do not reach in our sample. However, the fraction of objects with large EWs is small in Figure 5, and such objects would likely be missing in a smaller sample of Lyα emitters. This, in addition to the interpretations given by Ando et al. (2004), suggests that the trend seen at high redshift may be due to or enhanced by small-number statistics.

Figure 5 also allows us to identify ultraviolet luminous galaxies (UVLGs). This class of galaxies was defined by Heckman et al. (2005) among *GALEX* local galaxies as those that overlap the luminosity range of typical high-z LBGs. Using this definition, we have 11 UVLGs in our sample to the left of the dotted vertical line in Figure 5. These UVLGs do not have EWs as large as those found in less luminous objects. This is comparable, albeit at lower luminosity, with the trend reported for the high-z

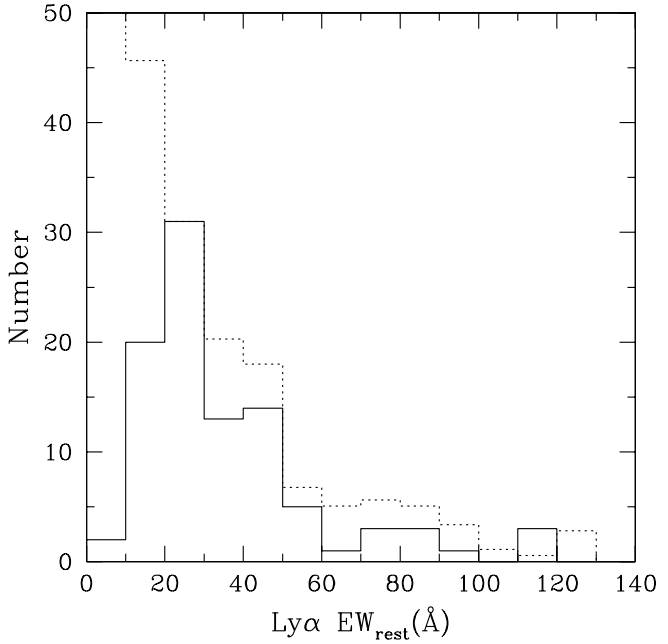

FIG. 3.—Distribution of Lyα rest-frame equivalent width (EW). The distribution of Shapley et al. (2003) is shown (*dotted line*) after a normalization with our data in the 20–30 Å bin.

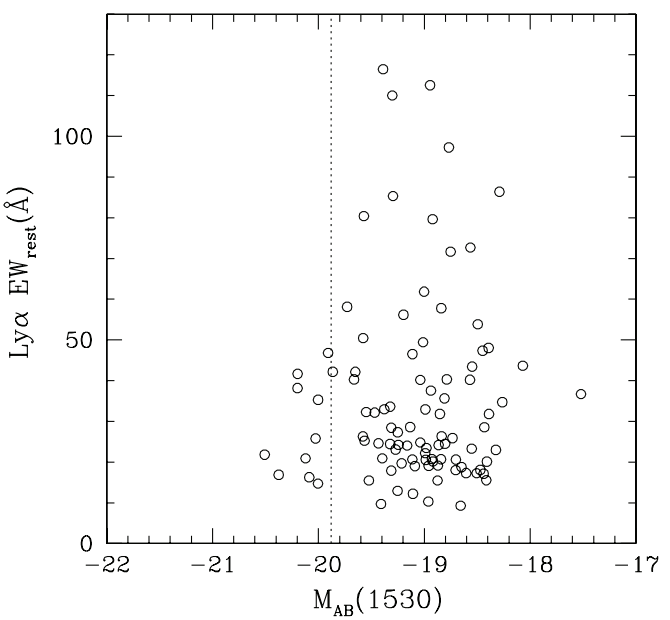

FIG. 5.—Lyα rest-frame EW as a function of the FUV absolute magnitude. The objects brighter than −19.9 (*vertical dotted line*) are UVLGs according to the definition of Heckman et al. (2005). The high-redshift galaxies discussed by Ando et al. (2004) are to the left of this line.

LBGs, and may also be explained by small-number statistics. Using the UV continuum LF obtained in the redshift range 0.2–0.4 by Arnouts et al. (2005), we calculate a density of UVLGs of about 2×10^{-5} Mpc^{-3}, and predict that about 24 of these objects will be in the redshift window $0.2 < z < 0.35$ and our five fields. With this evaluation, about 33% (8/24) of the UVLGs have Lyα in emission (with an EW larger than about 20 Å), which is a larger fraction than found above for the general population. Given the luminosity range of the UVLGs and the redshift window, incompleteness cannot explain that difference. In contrast, the evaluation of the number of luminous galaxies based on the bright end of the UV LF is uncertain. On the other hand, it is possible that a larger UV luminosity may contribute to a larger Lyα escape. This would be consistent, as would a possible evolution of the Lyα escape fraction, with the higher incidence of Lyα emission at higher redshifts reported by Reddy et al. (2008) and Ouchi et al. (2008).

3.4. *Lyα Dependences: Corollary Information*

Galaxy parameters not derived from *GALEX* observations are available for only a fraction of our relatively distant objects. An extreme example is the Hα line emission, which would allow us to derive the amount of ionizing radiation without the complication of resonant scattering and, therefore, the Lyα escape fraction. In spite of the 14 spectroscopic redshifts found in the literature (Table 2), we have been unable for various reasons (essentially lack of calibrated fluxes) to recover the Hα flux in more than two galaxies. The resulting Lyα/Hα ratios are found to be 19 (GROTH-21024), which is much above the theoretical recombination ratio of 8.7, and 5 (GROTH-34512), which is larger than any reported value in nearby star-forming galaxies (Giavalisco et al. 1996). These findings illustrate the difficulties of spectrophotometric comparisons and the need for a dedicated optical spectroscopic follow-up.

SDSS photometry (*ugriz* filters) is available for three of our five fields and 64 of our Lyα-emitting galaxy candidates. We have calculated the (NUV $-$ r) color, which has been extensively used by Wyder et al. (2007) in their study of galaxy colors with *GALEX* and is known to make a pronounced demarcation between the blue and red sequences. The range of colors obtained for our Lyα-emitting galaxy candidates is in good agreement with the values expected from galaxies. We find no trend between this color and the Lyα rest-frame EW, the Lyα-line luminosity, and the FUV luminosity. The ($u - r$) versus (NUV $-$ r) color-color diagram (Fig. 6) shows a sequence in good agreement with the blue part of the sequence (NUV $- r < 4$) obtained in the same diagram by Wyder et al. (2007) on a very large sample of galaxies (their Fig. 22). In contrast, the density of galaxies along our sequence is relatively constant, whereas it increases in the diagram of Wyder et al. (2007), with the (NUV $-$ r) color increasing from 0 to ~3. This difference probably results from the fact that we selected our objects from star-forming galaxies with a significant far-UV continuum and at redshift $z > 0.2$. We have separated the objects of Figure 6 into three groups according to their Lyα EW values. These categories do not appear to be segregated either along or perpendicular to the sequence, which is primarily driven, as suggested by Wyder et al. (2007), by star formation history. Since the Lyα EW (without any transfer) is predicted to be rather stable as a function of time in galaxies with constant star formation (Charlot & Fall 1993), this illustrates the dominant role of individual radiation transfer effects in the Lyα escape rather than stellar population properties (e.g., Schaerer & Verhamme 2008).

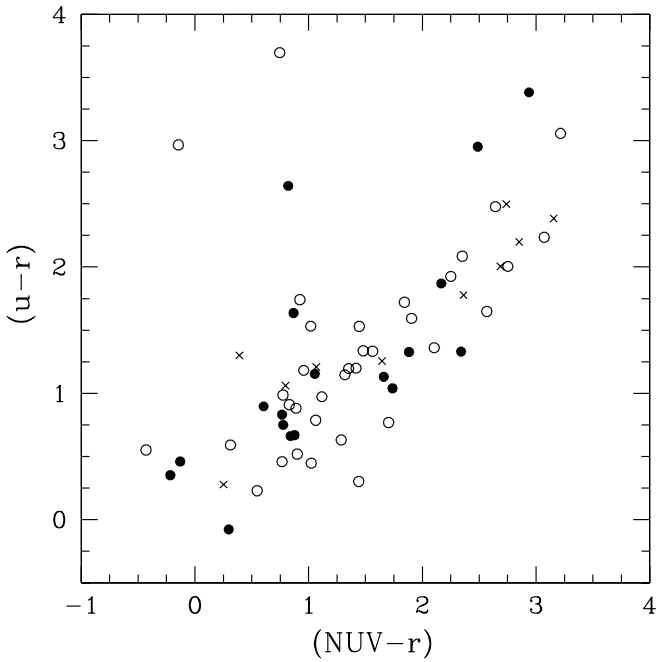

FIG. 6.—Color-color ($u - r$) vs. (NUV $-$ r) diagram built with the *GALEX* NUV flux and the SDSS flux measurements available for 64 of our Lyα-emitting galaxy candidates. One candidate with a low-quality emission feature and a ($u - r$) color about 6 σ out of the range expected from galaxies has been discarded. Different symbols are used according to the Lyα rest-frame EW: EW $<$ 30 Å (*open circles*), 30 Å $<$ EW $<$ 50 Å (*filled circles*), and EW $>$ 50 Å (*crosses*).

4. THE Lyα LUMINOSITY FUNCTION

4.1. *Volume Evaluation and Space Density*

For this approach, we need conditions of detection to be as uniform as possible. We have therefore restricted ourselves to the redshift range 0.2–0.35 and have retained only the objects of quality 1 or 2 in order to limit spurious detections. We have used the $V/V_{\rm max}$ method. For each Lyα-emitting galaxy candidate, $V_{\rm max}$ is the volume over which a source of the same Lyα luminosity could lie and still meet the blind search criteria. The inverse volumes of all the galaxies in a particular luminosity bin are summed to estimate the LF in that bin.

$V_{\rm max}$ is defined by the field of view and the redshift range 0.2–*zl*. The redshift *zl* is 0.35 if the Lyα luminosity is bright enough for the line to remain above the line-flux limit out to the upper bound of the redshift window. The corresponding volume, the maximum value of $V_{\rm max}$, is 2.369×10^5 Mpc^{-3}, taking into account a field-of-view radius of 0.6°. For fainter sources, *zl* is the redshift (<0.35) at which the Lyα flux falls below the line-flux limit. In this determination, the Lyα flux is decreased as the inverse square of the luminosity distance, since the Lyα is not spectrally resolved in the galaxies. The determination of *zl* is somewhat uncertain, since it is based on the line-flux limit, which is evaluated empirically in each field and results from both the depth of each field and the continuum level of the spectra. In practice, slight adjustments have been made to account for the specific noise in each spectra. Because of the relatively narrow redshift window, sources with a Lyα luminosity less than 10^{42} erg s^{-1} are the only ones that may be affected by these uncertainties in volume evaluation.

In order to combine the results obtained over the five fields, we have to deal with the differences in depth. Given the upper redshift limit of 0.35, the sources with Lyα luminosity $\log L >$ 41.8 (erg s^{-1}) are essentially above the line-flux limits in all

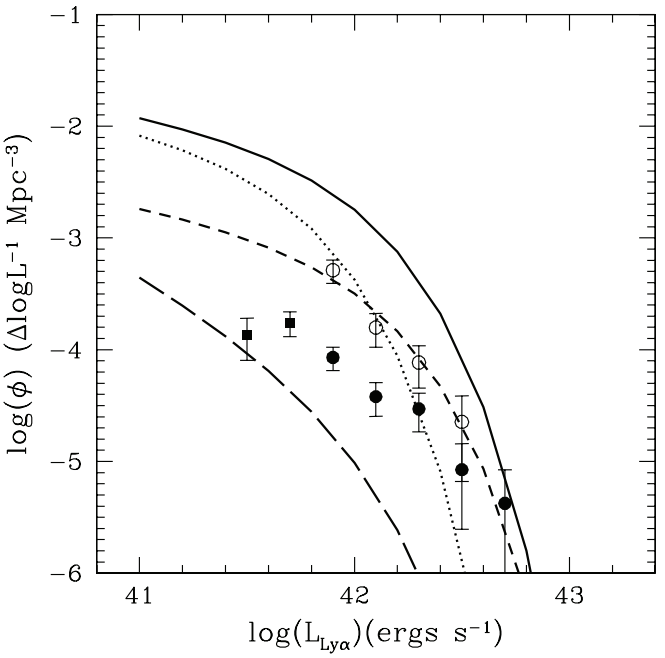

FIG. 7.—Space density of Lyα-emitting galaxies ($0.2 < z < 0.35$) per log $L_{\mathrm{Ly}\alpha}$ both as measured (*filled circles*, all five fields; *filled squares*, CDFS, GROTH, and NGPDWS fields) and with an evaluation accounting for incompleteness (*open circles*). The error bars are Poisson errors in our bins. LFs derived from the Hα LF of Tresse & Maddox (1998) are shown with Lyα/Hα = 1 for all galaxies (*solid line*), Lyα/Hα = 0.5 for all galaxies (*dotted line*), and a least-squares fit close to Lyα/Hα = 1 in 15% of galaxies (*short-dashed line*). An evaluation of the Lyα LF of narrow-line AGNs, derived from the Hα LF of Hao et al. (2005b), is displayed (*long-dashed line*) for comparison.

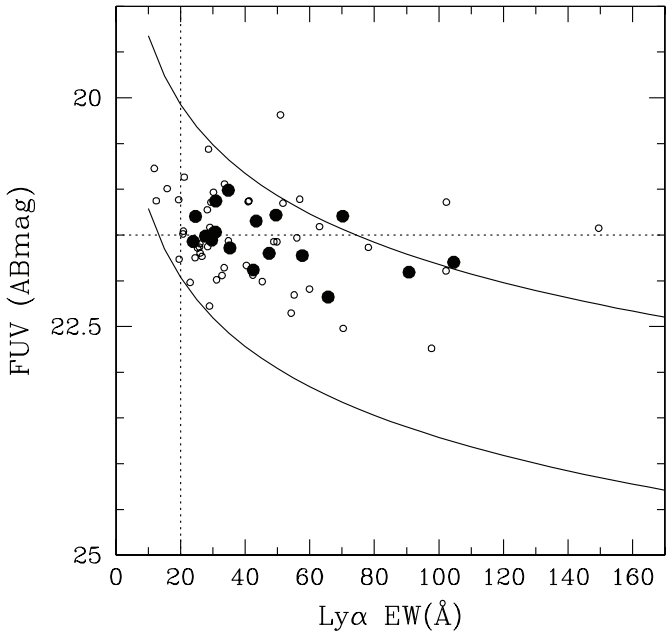

FIG. 8.—FUV (AB mag) flux vs. the Lyα EW. The objects from the Lyα luminosity bin 41.8–42.0 (log $L_{\mathrm{Ly}\alpha}$ in erg s^{-1}) lie between the two diagonal curves. In this domain, objects below the horizontal line at mag 21.5 may be missed because their continuum is too weak and their spectra not extracted; objects to the left of the vertical line may be missed because of a lack of contrast over the continuum. An evaluation of the resulting incompleteness is described in § 4.2. The observed data are overlaid (*circles*); the filled circles are the 18 objects of the luminosity bin 41.8–42.0. Two of these objects are slightly off the domain because of the average calibration factor involved in the calculation of their Lyα luminosity.

fields and can be reasonably merged. Adopting a bin width of 0.2 in log L, we have summed up the inverse volumes in their respective bins over the five fields and divided by 5 to account for the increased volume. It is possible to obtain the LF below the limit of log $L = 41.8$ (erg s^{-1}) at the expense of cosmic variance by using only the deepest three fields, CDFS, GROTH, and NGPDWS (cf Table 1). We have repeated the summations of inverse volumes over these three fields. The bin below log $L =$ 41.6 (erg s^{-1}) is again affected by incompleteness, and the lowest bin with only one source has been discarded as insignificant.

The resulting LF per log Lyα luminosity is plotted in Figure 7. As a generic consequence of detection thresholds in images, the lowest bins of the LF are affected by incompleteness. We have not tried to remedy this type of incompleteness and will only refrain from using the lowest luminosity bins in further discussion.

4.2. *Correction for Incompleteness*

In addition to the generic incompleteness accompanying the lowest bins of the LF, we have another source of incompleteness attached to the spectroscopic functionality of the grism images. The inclusion of a detected galaxy in the LF depends on the detection of the Lyα line. This source of incompleteness, which has no reason to be confined to the lowest luminosity bins, can take two aspects. First, a number of features with small equivalent widths may be missed because of a lack of contrast over the continuum flux; the distribution of EWs (similar to the distribution of rest-frame EWs in Fig. 3) shows that this happens below approximately EW = 20 Å. Second, objects with EWs larger than about 20 Å may be missed because their continuum flux is too low for a spectrum to be extracted; Figure 2 shows that spectra are not systematically extracted below a FUV magnitude of 21.5.

In order to understand the mechanisms of this second aspect of the incompleteness, we have illustrated the interplay between EW and observed FUV magnitudes in Figure 8. Because of the limited redshift range, each luminosity bin corresponds to a relatively narrow domain in this diagram. For example, Figure 8 shows the domain for the luminosity bin log $L_{\mathrm{Ly}\alpha} = 41.8$–42.0 (erg s^{-1}) between the two curves corresponding to Lyα line fluxes of 1.5 and 8.7×10^{-15} erg cm^{-2} s^{-1}. This domain is cut in two by the horizontal continuum flux limit at magnitude 21.5. In order to quantify the incompleteness, we first calculate the number of galaxies per 0.5 mag bin expected in our volume space as a function of UV magnitude. We use the LF obtained with the FUV band of *GALEX* by Arnouts et al. (2005) in the range $0.2 < z < 0.4$. In each 0.5 mag bin, the galaxies are in turn distributed in 10 Å EW bins according to the observed EW distribution (above the limit of 20 Å). This results in a number of Lyα-emitting galaxies for each elementary cell of size 0.5 mag and 10 Å EW in the diagram of Figure 8. These galaxy numbers per elementary cell can be summed over the domain defined above in Figure 8. The incompleteness factor is then taken as the ratio of the sum over the entire domain to the sum over the domain above the limit of 21.5 mag. If we account for the galaxies fainter than 21.5 mag that already contribute to the space densities plotted in Figure 7, we end up with an incompleteness factor of 6 for the luminosity bin log $L_{\mathrm{Ly}\alpha} = 41.8$–42.0 (erg s^{-1}), taken as an example in Figure 8.

We emphasize that this correction factor does not result from simulated data but only from an evaluation using the FUV LF, and that it relies on the assumption that the observed EW distribution of galaxies applies to the less-luminous galaxies involved in the evaluation. This assumption is supported by two facts. First, the observed EW distribution does not seem to change as a

function of the UV luminosity (Fig. 5), at least in the observed range. Second, the bulk of the correction factor originates from galaxies 1 or 1.5 mag fainter than the 21.5 mag limit, with EWs between 40 and 60 Å. This range of EW values seems less prone to change with luminosity than extreme values. As the uncertainties on the correction factor remain severe and the amplitude of the correction increases for the low-luminosity bins, we have repeated the evaluation only for the three luminosity bins brighter than 41.8–42.0, finding correction factors of 4.2, 2.6, and 2.7, respectively. The brightest bin, which corresponds to just one object, has not been corrected for. The space densities resulting from the incompleteness correction are plotted in Figure 7.

Figure 8 can also illustrate the other source of incompleteness resulting from small EW features that go undetected because of lack of contrast over the continuum; the relevant objects would lie in the domain defined by the two lines and the limit at EW < 20 Å. The EW distribution is essentially unknown in this area, but for all reasonable assumptions, an evaluation based on the same scheme as above leads to a negligible additional factor. This is due to the fact that galaxies are bright in this domain (at least those related to the high-luminosity bins) and are consequently much less dense than the faint galaxies involved in the first source of incompleteness described above.

4.3. *Comparisons with* Hα *Luminosity Functions*

Just as the comparison of the Lyα luminosity with the Hα luminosity of an individual star-forming galaxy places constraints on the escape of Lyα photons through the resonant scattering process, so we may compare the Lyα and the Hα LFs of galaxies. Since the escape of Lyα emission is expected to be highly variable from galaxy to galaxy, the comparison will lead to an average (Lyα-flux weighted) value of the escape, as if all galaxies were the same. For this comparison, we have used the Hα LF of Tresse & Maddox (1998) obtained at $z \sim 0.2$, which is close to our redshift window. This LF is itself consistent with other determinations (Tresse et al. 2002; Fujita et al. 2003; Nakamura et al. 2004). We adopt the values $\log L^* = 41.92$ erg s^{-1} and $\log \Phi^* = -2.56$ Mpc^{-3}, as updated from Tresse & Maddox (1998) to current cosmology ($H_0 = 70$ km s^{-1} Mpc^{-1}, $\Omega_\Lambda = 0.7$, $\Omega_m = 0.3$) by Fujita et al. (2003).

Because our binned data points are few and related to high luminosity values, we assume for our Lyα LF the same value $\alpha = -1.35$ as determined for the Hα LF. The Lyα/Hα ratio and the fraction of galaxies with Lyα emission are directly given by the modification factor for the parameters L^* and Φ^* that is necessary to fit our Lyα data. A change of L^* alone does not work well (see one example in Fig. 7), and a reasonable fit requires a decrease in Φ^*, which is equivalent to reducing the presence of Lyα in emission to only a fraction of the galaxies currently observed. Although systematic errors may be present in our completeness correction, we have carried out a least-squares fit on the five brightest luminosity data points, with L^* and Φ^* as free parameters. The fit (Fig. 7), given by $\log L^* = 41.98 \pm 0.09$ erg s^{-1} and $\log \Phi^* = -3.40 \pm 0.16$ Mpc^{-3}, implies a Lyα/Hα ratio of about 1 in 15% of the galaxies. As expected, the Lyα/Hα ratio is much lower than the ratio of 8.7 predicted by the case B recombination theory. This is in rough agreement with the range of values reported in nearby galaxies by Giavalisco et al. (1996) and implies an average Lyα escape fraction of about 0.1 somewhere between the average values of 0.02 and 0.8 in the galaxy formation models of Le Delliou et al. (2006) and Kobayashi et al. (2007), respectively.

At this stage, it is also possible to show that the Lyα LF is not affected by the fact that we have been unable to distinguish and remove narrow-line AGNs from our sample of Lyα-emitting galaxy candidates. We use the Hα LF of narrow-line AGNs derived from the SDSS by Hao et al. (2005b) with the criterion of Kauffmann et al. (2003), which gives the largest number of objects. The Lyα LF is derived with the Lyα/Hα ratio of 3.24 reported by Vanden Berk et al. (2001) from SDSS composite quasar spectra. The plot in Figure 7 shows that the contribution of narrow-line AGNs remains small, even if we account for some evolution between the redshift window of the SDSS sample (0–0.15) and ours (0.2–0.35).

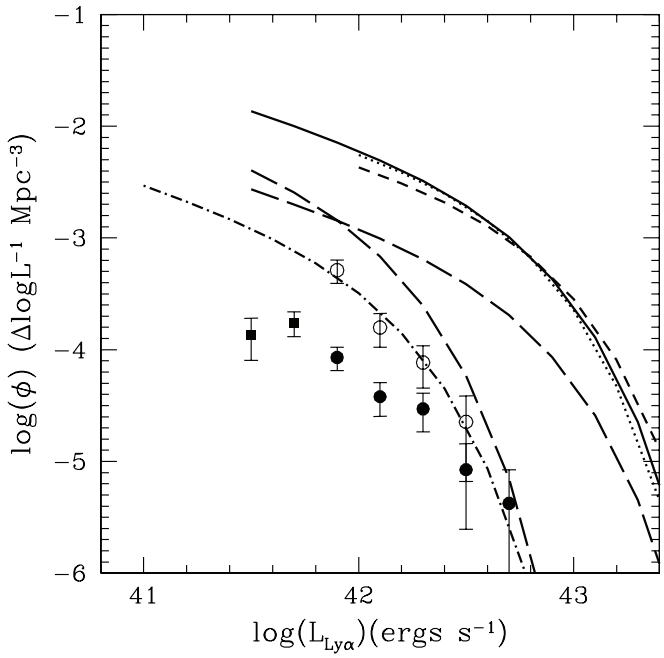

FIG. 9.—Space density of Lyα-emitting galaxies ($0.2 < z < 0.35$) per log $L_{\mathrm{Ly}\alpha}$ both as measured (*filled circles*, all five fields; *filled squares*, CDFS, GROTH, and NGPDWS fields) and with an evaluation accounting for incompleteness (*open circles*). The lines represent comparisons with Lyα LFs at high redshifts. *Solid line*: van Breukelen et al. (2005) at $2.3 < z < 4.6$ ($L^* = 5 \times 10^{42}$ erg s^{-1}, $\Phi^* = 0.0012$ Mpc^{-3}, $\alpha = -1.6$). *Dotted line*: Gronwall et al. (2007) at $z \sim 3.1$. *Short-dashed line*: Ouchi et al. (2008) at $z \sim 3.1$. The dot-dashed LF is derived from a least-squares fit on the 5 brightest points. The long-dashed lines show the impact of a factor of 5 decrease of L^* (the nearest curve to the data points) or Φ^* in the LF of van Breukelen et al. (2005); this factor corresponds to the decrease of the UV LD from $z \sim 3$ to $z \sim 0.3$.

4.4. *Comparisons with Ly*α *Luminosity Functions at High z*

It is interesting to compare the space densities of *GALEX* Lyα-emitting galaxies at $0.2 < z < 0.35$ with the Lyα LFs found at high redshift. In Figure 9, we have plotted the Lyα LF obtained by van Breukelen et al. (2005) at redshifts $2.3 < z < 4.6$, which we selected because it is the closest to our data in terms of redshift. In addition, the authors have compared their data with the measurements available at the time (see references in van Breukelen et al. 2005 and their Fig. 5). They conclude that the LF of Lyα emitters does not significantly change from $z \sim 3.4$ to $z = 5.7$. This is confirmed by more recent determinations from Ajiki et al. (2006), Tapken et al. (2006), Shimasaku et al. (2006), Murayama et al. (2007), Gronwall et al. (2007), Ouchi et al. (2008), and Dawson et al. (2007). A few LFs at $z > 6$ have been left out of the comparison because variations of Lyα LFs are possible that would not be related to the galaxies themselves, but to the IGM opacity resulting from changes in the IGM neutral fraction accompanying the reionization. Of the recent Lyα LFs at high redshift, we have elected for clarity to reproduce in Figure 9

only those closest to our redshift range, i.e., the two from Gronwall et al. (2007) and Ouchi et al. (2008) at $z = 3.1$.

Figure 9 shows that the space density of the Lyα-emitting galaxies is much lower in the range $0.2 < z < 0.35$ than at $z \sim 3$. We have quantified this factor by a least-squares fit on the five brightest data points, using the same α parameter (-1.6) as van Breukelen et al. (2005; adopted by these authors from Steidel et al. 1999); we have obtained $\log L^* = 42.03 \pm 0.08$ erg s^{-1} and $\log \Phi^* = -3.47 \pm 0.17$ Mpc^{-3}.

Compared to the values $L^* = (5 \pm 1.8) \times 10^{42}$ erg s^{-1} and $\Phi^* = 0.0012 \pm 0.0005$ Mpc^{-3} of van Breukelen et al. (2005), our determination implies a Lyα luminosity density (LD) $\sim$16.5 times larger at $z \sim 3$ than at $0.2 < z < 0.35$. In comparison, the FUV LD of Schiminovich et al. (2005) increases by a factor of about 5 between $z = 0.3$ and $z \sim 3$, an increase consistent with the compilations of star formation rate evolution of Hopkins (2004) and Hopkins & Beacom (2006). We have illustrated this difference in the evolution rates of the FUV and Lyα luminosity densities in Figure 9 by plotting the effect of a factor 5 decrease of the parameters L^* or Φ^* in the LF of van Breukelen et al. (2005). Although the effect looks significant, we now discuss further the uncertainties in our approach as well as possible interpretations.

1. Insofar as the FUV LD measures the evolution of the massive stellar content of the galaxies, the faster rate of evolution of the Lyα LD suggests a real increase (by a factor of about 3) of the Lyα escape fraction from $z \sim 0.3$ to $z \sim 3$. This is consistent with the observations of an increase with redshift of the fraction of (EW > 20) Lyα-emitting galaxies (this paper; Reddy et al. 2008). This is also consistent with the current idea that galactic winds are increasing with redshift, favoring the Lyα escape while mitigating the increased fraction of neutral hydrogen in galaxies at high redshift.

2. The rate of increase of the Lyα LD between $z = 0.3$ and $z \sim 3$ depends on the uncertainties of L^* and Φ^* at both redshifts, i.e., on four parameters. If we combine the variances obtained from our least-squares fit with those given by van Breukelen et al. (2005), the standard deviation on the factor 16.5 is as large as 11.5, and the evolution of the Lyα LD is faster than the FUV LD at a significance of about 84%.

3. A change in the faint-end slope α of the LF may play a role in the evolution of the Lyα LD, which is written $L^*\Phi^*\Gamma(\alpha + 2)$. The parameter α is indeed poorly constrained by the space densities of the luminous Lyα emitters that are observed both by *GALEX* and at high redshift. This parameter is assumed to be the same in our comparison between low and high redshifts. A steepening of the slope α at low z, resulting in an increase of $\Gamma(\alpha + 2)$, could make the evolution of the Lyα LD match that of the FUV LD. This would mean an increase of the Lyα escape fraction in low-luminosity objects at low z. Such a variation, however, would be opposite to the current trend of a steepening of the faint-end slope with redshift (e.g., Ryan et al. 2007 for FUV LF), as expected in the hierarchical formation scenario of galaxies.

In conclusion, the faster rate of evolution of the Lyα LD with respect to the cosmic star formation rate is significant at about 84% and probably indicates an increase of the average Lyα escape fraction from $z \sim 0.3$ to $z \sim 3$.

5. CONCLUSION

A blind search of potential Lyα emission features has been conducted on 7018 spectra obtained in five deep spectroscopic exposures with *GALEX*. We identified 96 Lyα-emitting galaxy candidates after a separation from AGNs carried out essentially on the basis of the FWHM. They are mostly in the redshift range 0.2–0.35. The following properties stand out.

1. The Lyα rest-frame equivalent-width distribution is comparable with that reported by Shapley et al. (2003) for LBGs at $z \sim 3$. The fraction of galaxies with Lyα emission (EW > 20 Å) seems smaller: 15% versus 25% in the LBG sample.

2. No trend is found between the EW and the (FUV $-$ NUV) color, in agreement with a decoupling of the reddening of line and continuum photons in Lyα resonant scattering. There is also no trend of the EW with the UV luminosity, except a decrease in a subsample of UVLGs. As at very high redshifts, small-number statistics might play a role here. A larger fraction of Lyα-emitting galaxies (EW > 20 Å) is found among UVLGs.

3. A subsample of 66 emission features of better quality and strictly in the redshift range 0.2–0.35 has been used to calculate the space densities of the Lyα-emitting galaxies. A scheme has been presented to correct for a major source of incompleteness, the fact that the spectra of objects with significant EWs may not have been extracted because their continuum is too weak.

4. A comparison with the Hα LF of Tresse & Maddox (1998) in the same redshift domain is consistent with an average Lyα-to-Hα ratio of 1 in about 15% of the galaxies.

5. A comparison of the Lyα LFs at $z \sim 0.3$ and $z \sim 3$ shows an evolution beyond that expected from the evolution of the massive stellar content of star-forming galaxies at a significance level of 84%, suggesting an increase of the average Lyα escape fraction with redshift.

GALEX (*Galaxy Evolution Explorer*) is a NASA Small Explorer, launched in 2003 April. We gratefully acknowledge NASA's support for construction, operation, and science analysis for the *GALEX* mission, developed in cooperation with the Centre National d'Etudes Spatiales of France and the Korean Ministry of Science and Technology. This research has made use of the NASA/IPAC Extragalactic Database (NED), which is operated by the Jet Propulsion Laboratory, California Institute of Technology, under contract with NASA.

REFERENCES

Ahn, S.-H., Lee, H.-W., & Lee, H. M. 2001, ApJ, 554, 604
———. 2002, ApJ, 567, 922
———. 2003, MNRAS, 340, 863
Ajiki, M., Mobasher, B., Taniguchi, Y., Shioya, Y., Nagao, T., Murayama, T., & Sasaki, S. S. 2006, ApJ, 638, 596
Ando, M., Ohta, K., Iwata, I., Watanabe, C., Tamura, N., Akiyama, M., & Aoki, K. 2004, ApJ, 610, 635
Ando, M., et al. 2006, ApJ, 645, L9
Arnouts, S., et al. 2005, ApJ, 619, L43
Charlot, S., & Fall, S. M. 1993, ApJ, 415, 580
Chen, W. L., & Neufeld, D. A. 1994, ApJ, 432, 567
Cowie, L. L., & Hu, E. M. 1998, AJ, 115, 1319
Davis, M., et al. 2007, ApJ, 660, L1
Dawson, S., Rhoads, J. E., Malhotra, S., Stern, D., Wang, J., Dey, A., Spinrad, H., & Jannuzi, B. T. 2007, ApJ, 671, 1227
Djorgovski, S., & Thompson, D. J. 1992, in IAU Symp. 149, The Stellar Populations of Galaxies, ed. B. Barbuy & A. Renzini (Dordrecht: Kluwer), 337
Finkelstein, S. L., Rhoads, J. E., Malhotra, S., Pirzkal, N., & Wang, J. 2007, ApJ, 660, 1023
Fujita, S. S., et al. 2003, ApJ, 586, L115
Giavalisco, M., Koratkar, A., & Calzetti, D. 1996, ApJ, 466, 831
Gronwall, C., et al. 2007, ApJ, 667, 79
Haiman, Z. 2002, ApJ, 576, L1

Hansen, M., & Oh, S. P. 2006, MNRAS, 367, 979
Hao, L., et al. 2005a, AJ, 129, 1783
———. 2005b, AJ, 129, 1795
Heckman, T. M., et al. 2005, ApJ, 619, L35
Hopkins, A. M. 2004, ApJ, 615, 209
Hopkins, A. M., & Beacom, J. F. 2006, ApJ, 651, 142
Hu, E. M., Cowie, L. L., & McMahon, R. G. 1998, ApJ, 502, L99
Kashikawa, N., et al. 2006, ApJ, 648, 7
Kauffmann, G., et al. 2003, MNRAS, 346, 1055
Kobayashi, M. A. R., Totani, T., & Nagashima, M. 2007, ApJ, 670, 919
Kunth, D., Mas-Hesse, J. M., Terlevich, E., Terlevich, R., Lequeux, J., & Fall, S. M. 1998, A&A, 334, 11
Le Delliou, M., Lacey, C. G., Baugh, C. M., & Morris, S. L. 2006, MNRAS, 365, 712
Malhotra, S., & Rhoads, J. E. 2004, ApJ, 617, L5
Martin, D. C., et al. 2005, ApJ, 619, L1
Mas-Hesse, J. M., Kunth, D., Tenorio-Tagle, G., Leitherer, C., Terlevich, R. J., & Terlevich, E. 2003, ApJ, 598, 858
Morrissey, P., et al. 2005, ApJ, 619, L7
———. 2007, ApJS, 173, 682
Murayama, T., et al. 2007, ApJS, 172, 523
Nakamura, O., Fukugita, M., Brinkmann, J., & Schneider, D. P. 2004, AJ, 127, 2511
Neufeld, D. A. 1991, ApJ, 370, L85
Ouchi, M., et al. 2008, ApJS, 176, 301
Pettini, M., Kellogg, M., Steidel, C. C., Dickinson, M., Adelberger, K. L., & Giavalisco, M. 1998, ApJ, 508, 539
Pettini, M., Steidel, C. C., Adelberger, K. L., Dickinson, M., & Giavalisco, M. 2000, ApJ, 528, 96
Reddy, N. A., Steidel, C. C., Pettini, M., Adelberger, K. L., Shapley, A. E., Erb, D. K., & Dickinson, M. 2008, ApJS, 175, 48
Ryan, R. E., et al. 2007, ApJ, 668, 839
Schaerer, D. 2007, preprint (arXiv:0706.0139)
Schaerer, D., & Verhamme, A. 2008, A&A, 480, 369
Schiminovich, D., et al. 2005, ApJ, 619, L47
Shapley, A. E., Steidel, C. C., Pettini, M., & Adelberger, K. L. 2003, ApJ, 588, 65
Shectman, S. A., Landy, S. D., Oemler, A., Tucker, D. L., Lin, H., Kirshner, R. P., & Schechter, P. L. 1996, ApJ, 470, 172
Shimasaku, K., et al. 2006, PASJ, 58, 313
Stanway, E. R., et al. 2007, MNRAS, 376, 727
Steidel, C. C., Adelberger, K. L., Giavalisco, M., Dickinson, M., & Pettini, M. 1999, ApJ, 519, 1
Stern, D., Yost, S. A., Eckart, M. E., Harrison, F. A., Helfand, D. J., Djorgovski, S. G., Malhotra, S., & Rhoads, J. E. 2005, ApJ, 619, 12
Tapken, C., et al. 2006, A&A, 455, 145
Tresse, L., & Maddox, S. J. 1998, ApJ, 495, 691
Tresse, L., Maddox, S. J., Le Fèvre, O., & Cuby, J.-G. 2002, MNRAS, 337, 369
van Breukelen, C., Jarvis, M. J., & Venemans, B. P. 2005, MNRAS, 359, 895
Vanden Berk, D. E., et al. 2001, AJ, 122, 549
Vanzella, E., et al. 2006, A&A, 454, 423
Verhamme, A., Schaerer, D., & Maselli, A. 2006, A&A, 460, 397
Way, M. J., Quintana, H., Infante, L., Lambas, D. G., & Muriel, H. 2005, AJ, 130, 2012
Weiner, B. J., et al. 2005, ApJ, 620, 595
Wolf, C., et al. 2004, A&A, 421, 913
Wyder, T. K., et al. 2007, ApJS, 173, 293
Xu, C. K., et al. 2005, ApJ, 619, L11